Appl. Phys. B 60, S241–S248 (1995)

Applied Physics B Lasers and Optics

© Springer-Verlag 1995

Phase locking of grating-tuned diode lasers

M. Prevedelli, T. Freegarde*, T.W. Hänsch

Max-Planck-Institut für Quantenoptik, D-85748 Garching bei München, Germany
(Fax: +49-89/32905-200, E-mail: MRP@zeus.ipp-garching.mpg.de)

Received: 2 September 1994 / Accepted: 6 September 1994

Abstract. We present a simple model for use in the design of reliable phase-locked loops for diode lasers, and a broad-range digital phase-frequency detector. By permitting a larger RMS phase error than analog detectors, the digital phase detector operates with a lower S/N ratio and locking bandwidth and allows very stable phase locking. Applications in optical frequency chains are discussed.

PACS: 42.55.Px; 42.62.Eh

Recent advances in high-resolution laser spectroscopy [1] have reinforced interest in the direct measurement of optical frequencies. Such measurements can be used to test basic theories, such as QED, to determine fundamental constants or to realize optical frequency standards. Frequency chains connecting optical secondary standards to interesting atomic transitions have already been realized [2, 3] or proposed [4].

One of the main limits to these experiments is the small number of secondary standards available. Usually, the frequency to be measured does not lie close enough to the harmonic of any standard. Large frequency differences may be coherently bridged using ultrafast detectors [5, 6], optical comb generators [7] and optical frequency dividers [8], but in each case and in particular in the latter, the complexity of the chain is increased, requiring several phase-locked sources. Diode lasers are particularly attractive for this purpose because they are inexpensive, small, and their frequency can be controlled by merely changing the injection current. In order to have a simple and compact optical setup, it is convenient to use lasers where the frequency is tuned and stabilized with an external diffraction grating. In comparison with cavity stabilized lasers [9], however, these sources have a broader linewidth and require a larger servo-bandwidth for stable phase locking.

Phase locking of diode lasers has already been achieved by a number of authors [10–13]. However, in most cases, the main goal was the quality of the lock (small RMS phase error) more than the simplicity and reliability of the setup. In a frequency chain, on the other hand, the final RMS phase error is likely to be dominated by the standard itself, while simplicity and reliability assume primary importance.

This paper is intended to be a practical guide for those who would like to build a simple and reliable OPLL for applications where residual phase noise is not critical. After a short discussion of basic principles, for readers unfamiliar with phase locking, we recall some equations from feedback theory, set our notation and derive several results for the shape of the beat note. Later we discuss a simple design procedure for an OPLL and a digital Phase and Frequency Detector (PFD) with a very broad (± 100 rad) phase detection range. The PFD is then compared with a traditional analog phase detector, showing that the larger RMS phase noise is compensated by greater reliability and less stringent requirements upon the minimum S/N ratio and loop bandwidth. Finally, the theory is compared with experimental results, showing that, for a typical frequency chain, it is possible to obtain good performance even with simple sources of rather broad linewidth.

1 Basic principles

Phase locking is used in frequency chains to transfer the definite frequency of a weak signal to a more powerful, tunable source. The transfer may either be direct so that the two frequencies are the same, or involve the addition of a third, usually rf, intermediate frequency. The latter is usually the more convenient, and often the more desirable.

Typically, in the first case, beams from the reference and slave lasers overlap on a photodiode, whose output depends upon the vector sum of the two field amplitudes and thus upon the phase difference between them, showing a roughly linear dependence for small errors. This is compared with a reference level corresponding to the desired phase difference, and the error is used to make a correction to the tunable slave laser. If a frequency-offset is required (second case), then the photodiode operates as a mixer and the resulting beat signal is compared with a reference of the required frequency using an electronic phase detector, whose output once again corresponds to the phase difference; it is this signal which is then fed back to the slave laser. The important feature, in

Dedicated to H. Walther on the occasion of his 60th birthday

* *Present address:* Physical Chemistry Laboratory, South Parks Road, Oxford OX1 3QZ, UK

relation to frequency chains, is that if the phase drift between the two sources is eliminated, then long term measurements of their frequencies must be the same.

In practice, the measurement time is finite, and the phase noise (related simply to the frequency noise) must be reduced to allow a frequency measurement of adequate precision. This is not, in practice, a major hurdle. Unfortunately, phase detectors operate correctly only within a finite range of phase error; beyond this, control is lost and a whole cycle, or a number of cycles, may "slip" between the reference and slave lasers in a manner analogous to a chain slipping the teeth of a cog. Since cycle-slipping leads directly to an error in frequency, the phase error must be kept well within the correct operating range of the phase detector. This requires the attenuation of not just the low-frequency noise, but also that up to quite high frequencies; this, in turn, requires the construction of fast servo loops, which can be a significant challenge.

Our approach has been to design a phase detector with a substantially increased range of operation, which thus tolerates a larger phase error for which slower stabilization circuitry is adequate.

2 A review of useful formulae

In this section we recall some formulae for later use. Detailed discussions of this subject are found in [14, 15] and references therein.

We will use lower case for time domain signals $s(t)$, and upper case for their Fourier transforms, $S(\nu)$, where $2\pi\nu = \omega$, and ω is the angular frequency. Since $s(t)$ is always real, $|S(\nu)|^2$ is an even function of ν. If $c_f(t)$ and $P_f(\nu)$ are the correlation function and the power spectral density for the quantity f, it is convenient to use the single–sided power spectral density, defined for $\nu > 0$ as $P_f^1(\nu) = P_f(\nu) + P_f(-\nu) = 2P_f(\nu), P_f^1(-\nu) = 0$; in most experimental situations negative frequencies cannot be measured, but their contribution to $P_f(\nu)$ is folded on the positive axis. The Wiener-Khintchine theorem then takes the form [14]:

$$P_f^1(\nu) = 4\int_0^\infty c_f(t)\cos(2\pi\nu t)\,dt\ , \tag{1}$$

$$c_f(t) = \int_0^\infty P_f^1(\nu)\cos(2\pi\nu t)\,d\nu\ . \tag{2}$$

A typical OPLL is composed of a Master Laser (ML), a Slave Laser (SL), a Local Oscillator (LO), and a feedback loop. The phase of the beat note between the two lasers is compared with the phase of the LO and the derived error signal is used to control the frequency of the SL. This system can be described by standard feedback theory assuming the instantaneous frequency difference between the beat note and the LO to be the input variable $i(t)$.

In our model, we consider a feedback loop composed of four parts: a phase detector, a delay, a loop filter, and the slave laser. If the Fourier transforms of the loop filter and of the SL response are $L(\nu)$ and $D(\nu)$, then we can write the Fourier transform of the output $o(t)$ as:

$$O(\nu) = \frac{I(\nu)}{1+G(\nu)}\ , \tag{3}$$

where

$$G(\nu) = D(\nu)\,L(\nu)\,\exp(-2\pi\mathrm{i}\,\nu\tau)\,\frac{G_p}{2\pi\mathrm{i}\nu}\ . \tag{4}$$

Here, τ is the delay of the feedback loop and G_p is the gain of the phase detector, measured in V/rad. The explicit form of $D(\nu)$ and $L(\nu)$ will be discussed in Sect. 4.

If $O(\nu)$ is known, it is possible to derive other useful quantities. We will need the mean-square phase error $\langle\varphi^2\rangle$ [here, $\langle\,\rangle$ denotes the time average and $\varphi(t)$ is the integral with respect to time of $o(t)$] and the Allan variance $\sigma^2(t)$:

$$\langle\varphi^2\rangle = 2\int_0^\infty \frac{|O(\nu)|^2}{(2\pi\nu)^2}\,d\nu\ , \tag{5}$$

$$\sigma^2(t) = 4\int_0^\infty \frac{|O(\nu)|^2}{(2\pi)^2}\,\frac{\sin^4(\pi\nu t)}{(\pi\nu t)^2}\,d\nu\ . \tag{6}$$

Equation (6) does not define $\sigma^2(t)$ in terms of the normalized frequency y; the more conventional $\sigma_y^2(t)$ is obtained by dividing our value by the square of the laser frequency.

Another commonly measured function is the power spectrum $P_\varphi(\nu)$ of the beat note (the rf power spectrum). Since this is the only power spectrum we will use, we shall drop the index φ. We note, that if $c_\varphi(t)$ is the correlation function for $\varphi(t)$, the function $r(t) = c_\varphi(t) - c_\varphi(0)$ is given by:

$$r(t) = -4\int_0^\infty \frac{|O(\nu)|^2}{(2\pi\nu)^2}\,\sin^2(\pi\nu t)\,d\nu\ . \tag{7}$$

Recalling that, if $\varphi(t)$ describes a Gaussian process [15],

$$\langle\exp[\mathrm{i}\varphi(t'+t) - \mathrm{i}\varphi(t')]\rangle = \exp[r(t)]\ , \tag{8}$$

we can apply the Wiener–Khintchine theorem to obtain:

$$P(\nu-\nu_0) = 2\int_0^\infty \exp[r(t)]\cos(2\pi\nu t)\,dt\ , \tag{9}$$

where ν_0 is the LO frequency. Equation (9) cannot be solved generally, so we shall use an approximate relation between $|O(\nu)|^2$ and $P(\nu-\nu_0)$. It can be shown [16] that for $\langle\varphi^2\rangle < 1$ and $|\nu-\nu_0| > \Delta$, where Δ is the HWHM of $P(\nu-\nu_0)$,

$$P(\nu-\nu_0) \sim |\Phi(\nu)|^2 = \frac{|O(\nu)|^2}{(2\pi\nu)^2}\ . \tag{10}$$

We also define the fraction of power in the carrier, $\eta = P(0)/(\int_{-\infty}^{+\infty} P(\nu)d\nu)$. If $\langle\varphi^2\rangle \ll 1$ then

$$\eta = \exp(-\langle\varphi^2\rangle)\ . \tag{11}$$

In practice, the value of η from (11) is used as a figure of merit even when $\langle\varphi^2\rangle \approx 1$.

3 Calculation of the rf power spectrum

In this section, we use (7), (9) and (10) to derive some results regarding $P(\nu-\nu_0)$ for free-running and weakly locked diode lasers (weakly locked meaning that the servo-bandwidth is much narrower than the beat note) in the presence of white, $1/f$, and Lorentzian frequency noise. We assume

$$|I(\nu)|^2 = (2\pi)^2 \left(S_w + \frac{S_{1/f}}{2\pi\nu} + S_L \frac{\nu_L^2}{\nu^2 + \nu_L^2} \right) , \quad (12)$$

where the factor $(2\pi)^2$ gives the noise spectral densities S_i in Hz^2/Hz. For the free-running case $|I(\nu)|^2 = |O(\nu)|^2$. For a weak lock we can neglect the delay and assume that $L(\nu)$ and $D(\nu)$ are constant in (4). If $G(\nu) = \nu_u/i\nu$, where ν_u is the unity-gain frequency, then

$$|O(\nu)|^2 = |I(\nu)|^2 \frac{\nu^2}{\nu^2 + \nu_u^2} . \quad (13)$$

We first discuss the case of pure white noise. For the free-running case, $P(\nu - \nu_0)$ will be a Lorentzian with HWHM $\Gamma = \pi S_w$. Alternatively, in terms of the single sided power density S_w^1, $\Gamma = \pi S_w^1/2$. In the presence of feedback, expanding $\exp[r(t)]$ in (9), integrating term by term, and finally setting, from (5), $\langle\varphi^2\rangle = \pi S_w/\nu_u$ we obtain:

$$P(\nu - \nu_0) = \exp(-\langle\varphi^2\rangle) \times \left[\delta(\nu - \nu_0) + \frac{1}{\pi} \sum_{n=1}^{\infty} \frac{\langle\varphi^2\rangle^n}{n!} \frac{\nu_u n}{(\nu_u n)^2 + (\nu - \nu_0)^2} \right] . \quad (14)$$

The line shape is composed of a δ-function and a pedestal, which is a series of Lorentzians. The series can be written in terms of the confluent hypergeometric function ${}_1F_1(a, b, z)$ as

$$\frac{1}{\pi} \sum_{n=1}^{\infty} \frac{\langle\varphi^2\rangle^n}{n!} \frac{\nu_u n}{(\nu_u n)^2 + (\nu - \nu_0)^2} = \frac{\langle\varphi^2\rangle}{\pi\nu_u} \left(\frac{{}_1F_1(1 - i\theta_u, 2 - i\theta_u, \langle\varphi^2\rangle)}{1 - i\theta_u} + \text{c.c.} \right) , \quad (15)$$

with $\theta_u = (\nu - \nu_0)/\nu_u$. Using the asymptotic expansions for ${}_1F_1(a, b, z)$, it can be shown, that when $(\nu - \nu_0) \gg \nu_u$ or when $(\nu - \nu_0) < \Gamma$ and $\nu_u \ll \Gamma$, then $P(\nu - \nu_0)$ tends towards the expected Lorentzian with a HWHM of $\Gamma = \pi S_w$.

Direct integration of (14) shows that the fraction η of power in the δ-function is given by (11). The contribution of the series to $P(0)$ is $[\exp(-\langle\varphi^2\rangle) - 1]/\pi\nu_u$ and can be neglected when $\langle\varphi^2\rangle \ll 1$.

The free-running linewidth in the presence of white and Lorentzian noise can similarly be written as:

$$P(\nu - \nu_0) = \frac{\exp(S_L\pi/\nu_L)}{\pi} \sum_{n=0}^{\infty} \frac{1}{n!} \left(-\frac{S_L\pi}{\nu_L} \right)^n \times \frac{\pi(S_w + S_L) + n\nu_L}{[\pi(S_w + S_L) + n\nu_L]^2 + (\nu - \nu_0)^2} , \quad (16)$$

or, with $\theta_{wL} = (\nu - \nu_0)/\nu_L$, $u = S_L\pi/\nu_L$, and $v = \pi(S_w + S_L)/\nu_L$,

$$P(\nu - \nu_0) = \frac{1}{\pi\nu_L} \left(\frac{{}_1F_1(1, v + i\theta_{wL} + 1, u)}{v + i\theta_{wL}} + \text{c.c.} \right) . \quad (17)$$

The importance of the low-frequency noise is controlled by u. When $u \ll 1$, $P(\nu - \nu_0)$ tends to a Lorentzian with $\Gamma = \pi(S_w + S_L)$, while for $u \gg 1$, the limit is again a Lorentzian and $\Gamma = \pi S_w$.

We do not try to solve the problem in presence of feedback. In most cases, however, it is possible to use the results for white frequency noise by choosing the proper effective S_w, depending on the value of u.

If $1/f$ noise is considered, the integral in (7) diverges at $\nu = 0$ for the free-running case. A low-frequency cut–off at $\nu = \nu_c$ must be then introduced, which can be justified in terms of a finite measurement time. After further approximations, the final result is a Gaussian with a HWHM that depends on ν_c [17]. To derive a relation between the HWHM of the power spectrum and $S_{1/f}$, however, it is possible to use (10). Following [18], we will assume

$$P(\nu - \nu_0) = C(\mu) \left(\frac{a^2}{a^2 + (\nu - \nu_0)^2} \right)^{\mu} , \quad (18)$$

where $C(\mu)$ is the normalization constant, so that the total power is equal to 1:

$$C(\mu) = \frac{\Gamma(\mu)}{a\,\Gamma(1/2)\,\Gamma(\mu - 1/2)} . \quad (19)$$

From (10), we obtain, for $(\nu - \nu_0) > a$,

$$|I(\nu)|^2 \simeq (2\pi)^2 C(\mu) \frac{a^{2\mu-1}}{\nu^{2\mu-2}} . \quad (20)$$

In the case of $1/f$ noise, we then have $\mu = 3/2$ and $S_{1/f} = \pi a^2$. The relation between a and the HWHM Δ is $\Delta = a\sqrt{2^{(2/3)} - 1}$.

If feedback is applied, we may assume the same form for the rf spectrum, but let $\nu_c \simeq \nu_u$.

4 A model for the loop

To determine the output spectrum $O(\nu)$, we must measure and make assumptions about the parameters and the functions that appear in (4). Specifically, we start with a preliminary hypothesis about the laser response $D(\nu)$ and measure all the other parameters while keeping the loop-filter characteristics $L(\nu)$ constant. We then try to design the optimum $L(\nu)$ under certain constraints. A description of the experimental techniques used for measuring the loop parameters of our diodes will be given in Sect. 6. Once $O(\nu)$ is known we can evaluate $\langle\varphi^2\rangle$ and $\sigma(t)$ for our loop using (5, 6).

We are interested in $D(\nu)$ only up to frequencies of the order of the loop bandwidth, typically less than 10 MHz. It is generally assumed [17] that in this region the physical mechanism responsible for FM modulation is the variation of the refractive index inside the diode-laser chip due to the temperature change induced by the current, and in the region of interest the response can be approximated by a single-pole fall–off corresponding to a thermal time constant of a few microseconds,

$$D(\nu) = G_d \frac{\alpha}{i\nu + \alpha} . \quad (21)$$

The actual values of α and G_d must be measured directly. Typically, α is 100 kHz to 1 MHz and G_d is 1 GHz/mA.

To determine the free-running power spectrum $|I(\nu)|^2$, we have measured the beat note (Fig. 1), between two identical, weakly locked, grating-stabilized diode lasers and used the results of Sect. 3. Fitting a pure Lorentzian shows that white frequency noise is a poor model and excess noise must be added below 1–2 MHz in order to fit the rf spectrum. This will be discussed in Sect. 6.

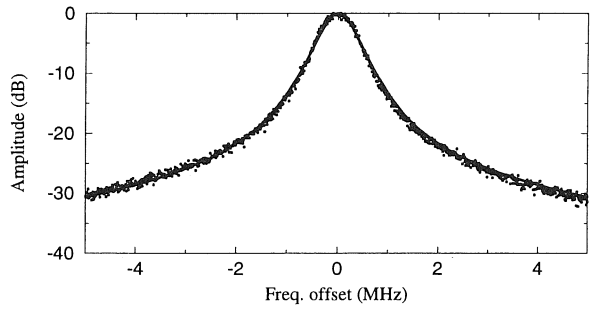

Fig. 1. Beat note between two identical grating-stabilized diode lasers (average of 100 scans, resolution bandwidth 10 kHz, locking bandwidth 30 kHz). The *solid line* is a fitted form, assuming a Lorentzian and white noise

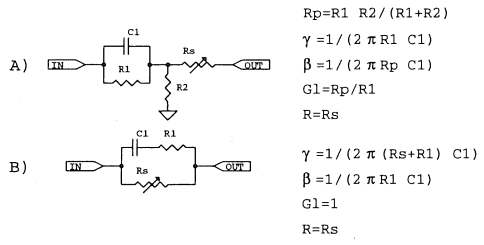

Fig. 2. A pair of loop filters implementing the transfer function in (22)

To evaluate the loop bandwidth, unity gain, and phase margin, we need to consider the frequency range where $|G(\nu)|^2 \simeq 1$, which is usually above 2 MHz. We will assume $|I(\nu)|^2$ to be constant in this region.

The simplest passive filter that allows us to widen our loop bandwidth has the following transfer function:

$$L(\nu) = \frac{G_1}{R}\frac{\beta}{\gamma}\frac{\mathrm{i}\nu+\gamma}{\mathrm{i}\nu+\beta}\ , \tag{22}$$

where $\gamma < \beta$, $G_1 \leq 1$, and R is the resistor used for voltage to current conversion. Figure 2 shows two possible implementations: the first is the standard phase-advance circuit followed by R, while the second produces a current output directly. The relations between the parameters in (22) and the values of the components are added for convenience.

If we set $\gamma = \alpha$ and $\beta \gg 1/2\pi\tau$, (4) can be approximated, for $\nu < 1/2\pi\tau$, by:

$$G(\nu) = \nu_u \frac{\exp(-2\mathrm{i}\pi\nu\tau)}{\mathrm{i}\nu}\ , \tag{23}$$

where $\nu_u = G_d G_1 G_p / 2\pi R$ is the unity-gain frequency. In practice, since β can increase the loop noise, it should not exceed 3–5 times $1/2\pi\tau$.

The maximum loop bandwidth is limited by the phase shift due to the delay. If we want a phase margin of about 30 degrees, we can set $\nu_u = 1/2\pi\tau$, while the gain margin is $20\log(\pi/2) \simeq 4$ dB. For a more precise calculation, (4) and a better model for $|I(\nu)|^2$ should be used.

A crude estimate of the phase error can be made, neglecting low-frequency noise, letting $\langle\varphi^2\rangle = S_w \tau I_1$, where:

$$I_1 = 2\int_0^\infty \frac{1}{x^2 - 2x\sin(x) + 1}\,dx \approx 10.72\ . \tag{24}$$

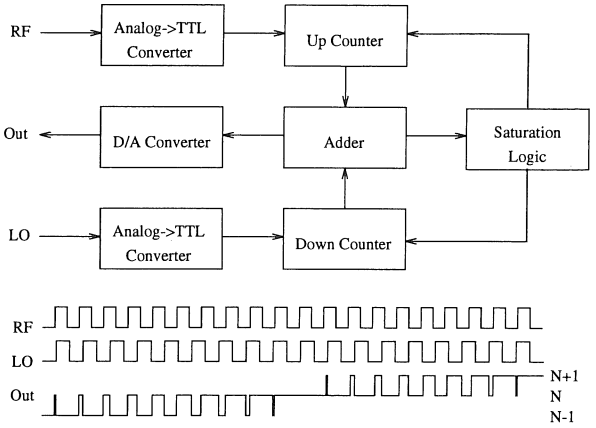

Fig. 3. Block diagram of the digital PFD. The timing diagram shows the PFD output, with the adder initially storing N–1, for a rf frequency 10% greater than the LO frequency

We could compute $\sigma(t)$ numerically but, for our purposes, a simple approximation will suffice. We expand $\sin^4 \pi\nu t$ in (6) as an average value and two oscillating terms; since we are interested in values of t for which $t \ll \tau$, the contribution of the oscillating terms is negligible. We then have:

$$\sigma^2(t) \simeq \frac{3}{(2\pi t)^2}\langle\varphi^2\rangle\ . \tag{25}$$

This holds only if $|O(\nu)|^2/\nu^2$ does not diverge at $\nu = 0$.

If the loop is not ideal, but has an internal noise source $n(t)$, (3) becomes:

$$O(\nu) = \frac{I(\nu)}{1+G(\nu)} + \frac{N(\nu)G(\nu)}{1+G(\nu)}\ . \tag{26}$$

The noise is faithfully superimposed on $O(\nu)$ by the feedback loop, since it is interpreted as an error signal. The most common kind of noise is white phase noise due to the finite S/N ratio of the beat note. A simple assumption is to set $2\pi\nu\,|N(\nu)| \simeq 1/r$, where r is the S/N ratio in 1 Hz bandwidth.

With $G(\nu)$ as in (23) and $|I(\nu)|^2 = (2\pi)^2 S_w$ we obtain:

$$\langle\varphi^2\rangle = I_1\left(S_w\tau + \frac{1}{r^2\tau}\right)\ , \tag{27}$$

showing that, if noise is included, there is an optimum bandwidth which minimizes $\langle\varphi^2\rangle$, giving $\langle\varphi^2\rangle$ with respect to τ as $2I_1\sqrt{S_w/r^2}$ at $\tau = 1/\sqrt{r^2 S_w}$. In practice, however, both S_w and τ are given and ν_u is determined by the required phase or gain margin. One can only be careful and check that the main contribution to $\langle\varphi^2\rangle$ comes from the first term in (27).

5 Non-ideal phase detectors

So far we have assumed a perfect Phase Detector (PD), i.e., a device whose output is proportional to $\varphi(t)$. This is not realistic: when the lasers are in lock, the phase error will not vary by more than a fraction of a radian, but, as soon as the SL goes out of lock, φ can easily vary at a rate of 10^8

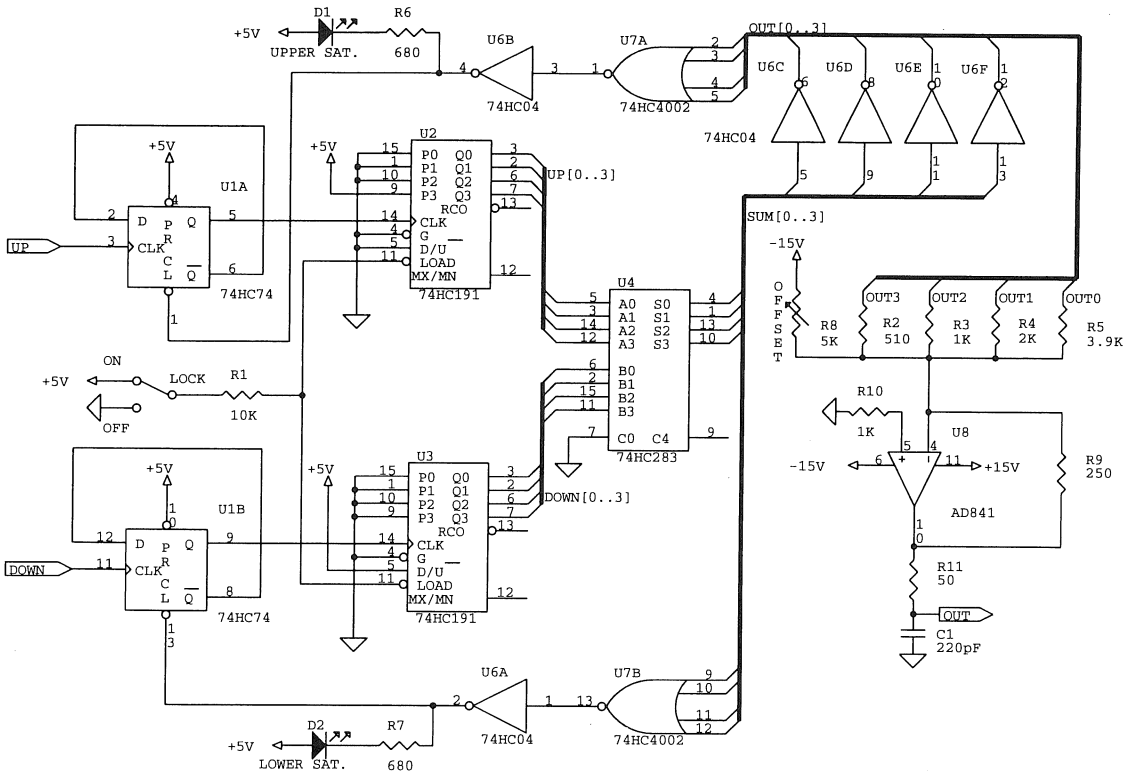

Fig. 4. Electrical scheme of the digital PFD. The analog–to–TTL converters and the analog front-end after the DAC are not shown

rad/s. Any practical PD should, therefore, reach a limiting output, indicating in which direction the phase is growing. This constant voltage can then be used by some slow control system (e.g., the PZT driver of the SL) to relock the lasers.

The most common kind of PD, the analog mixer, has an output proportional to $\sin \varphi(t)$; it is monotonic for only π rad and can be assumed linear only for $\varphi < 1$ rad. Beyond the monotonic range, it does not saturate but reverses sign. These poor characteristics mean that, unless $\langle \varphi^2 \rangle$ is kept very small, there will be a significant probability of the instantaneous value of $\varphi(t)$ exceeding $\pi/2$; this will change the sign of the feedback signal and lead eventually to a cycle slip. Computing the average time between two cycle slips t_s is not easy [19] but a simple expression can be stated [4] for a first-order loop:

$$t_s = \frac{\pi \exp\left(2/\langle \varphi^2 \rangle\right)}{4\nu_u} . \tag{28}$$

It is clear that, when $\langle \varphi^2 \rangle \simeq 1$, the frequency error due to cycle slips is too large for a frequency chain, even though $\sigma^2(t)$ in (25) is a fraction of a Hz at $t = 1$ s. For broad sources, then, it would be very useful to remove this limitation.

Digital PDs can easily provide a linear output and wider phase-detection range. Converting the beat note and the LO signal to digital levels and applying them to the inputs of an XOR gate gives, after a low-pass filter, a linear PD with the same monotonic range as an analog one. Dividing both signals by n before the XOR increases the range to $n\pi$. Saturation can then be obtained with some extra components and, indeed, single-chip devices implementing a 4π Phase and Frequency Detector (PFD) are available.

A dividing PFD, however, increases the implicit loop delay, limiting the maximum loop bandwidth. We define the implicit delay as $\tau_i = 1/\nu_0$. It is easy to see why any product detector used as a PD forces a minimum delay: the useful information is contained in the difference signal, while the sum must be filtered out by a low-pass filter with a corner frequency of the order of ν_0. Expanding its transfer function to first order in ν/ν_0 shows that this filter is equivalent to a delay τ_i for $\nu/\nu_0 \ll 1$. A digital PD can sense only toggles of the input signals and, therefore, measures the beat-note phase every half cycle of the LO. If images are to be rejected, according to the sampling theorem, the bandwidth must be limited to ν_0. This fixes τ_i. Moreover, we have not only an upper limit on the loop bandwidth but also a true delay; on average we must wait a quarter of a cycle of the LO frequency before detecting a phase variation.

Another possible digital PD [20], is a simple "phase counter": we add +1 (−1) to a register for each cycle of the beat note (LO). The register value is then converted to an analog signal and filtered. Since a simple counter with up and down clock inputs will not operate properly in the presence of "simultaneous" transitions, the safest way to achieve this is to sum the outputs of an up–counter connected to the beat note and a down–counter connected to the LO (Fig. 3). The linear range is limited only by the number of bits in the counters and the adder; saturation is accomplished by recognizing the "all zeroes" and "all ones" states at the adder output and blocking the input of the appropriate counter. A

typical timing diagram is shown in the lower part of Fig. 3; it is apparent that this circuit not only correctly counts whole cycles of phase error, but with suitable filtering at the output also gives an appropriate linear response.

Our circuit, using 6 standard TTL ICs (Fig. 4), has 5 bit counters (a D–type flip–flop plus a 4 bit synchronous counter) and a 4 bit adder. The linear range is then $\pm 32\pi$ (about ± 100 rad). The DAC is simply 4 resistors and an OP–AMP. The sensitivity is 25 mV/rad and the delay due to the electronics is about 50 ns including the analog–to–TTL converter. The maximum LO frequency is 70 MHz and is limited by our converter; with faster components (using ECL logic) this could be extended up to 200 MHz.

Additional advantages of this digital PFD, in comparison with an analog one are: calibrated sensitivity, broader capture range and sideband selection (an analog mixer can lock the SL at $\pm\nu_0$ from the ML, which cannot happen with this PFD). On the other hand, a digital PFD will always be slower (higher τ_1) and noisier since it is sensitive only to the edges of the input signals and not to the average integrated over one period.

6 Experimental results

For our experiments, we have used MQW diode lasers (STC, model LT50A-03U) at 850 nm, stabilized with optical feedback from a 1800 lines/mm grating, placed 15 mm from the laser, mounted in Littrow configuration. The divergence of the beam is compensated with a collimating lens giving a numerical aperture of 0.45. The typical threshold current I_T is about 32 mA and the operating current is between 50 and 60 mA. The temperature of the diode is stabilized to within 1 mK using a Peltier element. In order to avoid unwanted optical feedback, a double-stage optical diode providing 60 dB of isolation is used for each laser. After being combined at a beam splitter, the ML and the SL beams are focused onto an avalanche photodiode and the resulting signal is then amplified by 54 dB using two cascaded amplifiers. The LO signal is provided by a rf synthesizer.

As a phase detector, we have used both an analog mixer and the digital PFD. The output of the PD is split into two paths: the first is used to control the injection current via the loop filter; the second is directed, after an integrator, to a low voltage PZT used to tilt the grating. This part of the loop provides a dc-coupled feedback path, allowing broad frequency tunability. The setup is illustrated in Fig. 5.

The power spectrum of the beat note between two identical grating-stabilized diode lasers is shown in Fig. 1. The lasers were weakly locked, using the digital PFD and just a resistor as the loop filter, giving a loop bandwidth of $\approx$30 kHz. The data are the average of 100 scans of the spectrum analyzer. The FWHM of the rf spectrum is 570 kHz. A fit with a simple Lorentzian does not give a satisfactory result, showing that the spectrum is broadened by low-frequency noise. Better agreement is obtained either by fitting a Lorentzian in the wings only and (18), with $\mu = 3/2$, up to $\simeq$ 2 MHz ($1/f$ low-frequency noise), or by using (17) (Lorentzian low-frequency noise). In the first case, we obtain $S_w = 48 \times 10^3$ Hz^2/Hz and $S_{1/f} = 0.43 \times 10^{12}$ Hz^2, so that the $1/f$ corner is at about 1.4 MHz. In the second,

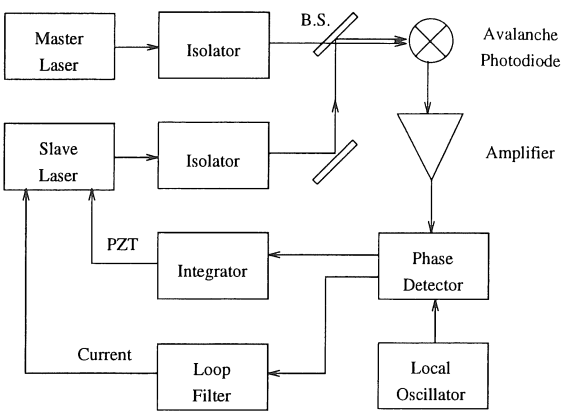

Fig. 5. Experimental setup of the OPLL

$S_w = 25 \times 10^3$ Hz^2/Hz, $S_L = 100 \times 10^3$ Hz^2/Hz while it has been assumed $\nu_L = \alpha = 400$ kHz (see next paragraph), since Lorentzian low-frequency noise can be thought of as external white noise (i.e., current fluctuations) filtered by $D(\nu)$. The second set of parameters allows an easier comparison with the experimental data, since it does not require the introduction of a low-frequency cut–off, and is our preferred choice. The rf spectrum calculated in this way is also shown in Fig. 1.

The FM response $D(\nu)$ has been measured in two different ways. In the first experiment a solitary laser (without grating) was tuned to the side of a Cs absorption line, and the intensity modulation of the laser beam measured as a function of the injection-current modulation using a network analyzer for frequencies up to 50 MHz. A similar measurement away from resonance allowed the AM response to be determined, and hence the pure FM transfer function to be derived. The results, after correction for the photodiode response, cable length and diode laser input network are shown in Fig. 6. In the second experiment, two grating-tuned lasers have been phase locked with a small servo bandwidth. By measuring the output of the PFD versus current modulation of the master laser we have obtained another estimate for $D(\nu)$. In both cases, we obtained a corner frequency α between 350 and 400 kHz.

G_d has been measured by simply tuning the current and observing the laser output with a scanning Fabry–Perot: $G_d = 800$ MHz/mA. If we assume that S_L is due to current noise, we derive a very reasonable value of 0.4 nA/$\sqrt{\text{Hz}}$ for the current noise density of the power supply.

Our estimate for the delay was $\tau \approx 20$ ns for the analog PD and $\tau \approx 90$ ns for the digital circuit. With these numbers, we have then designed loops for both an analog and a digital PD, according to the procedure described in Sect. 4.

For the analog PD, using a mixer with a sensitivity of about 460 mV/rad and a LO frequency of 50 MHz, we have used a loop filter as in Fig. 7 with a loop bandwidth of about 8 MHz. The recorded beat note is shown in Fig. 8. We have measured η from direct integration of the data in Fig. 8 for frequencies up to 25 MHz from the carrier. Since, for higher frequencies, $|O(\nu)|^2 \simeq |I(\nu)|^2$, the power in the wings can be estimated by simply integrating a Lorentzian. Letting

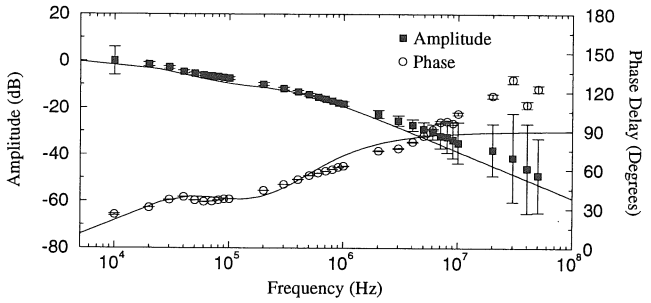

Fig. 6. Injection current FM phase and amplitude response for a free-running laser. The *solid lines* were computed assuming a zero at 70 kHz and two poles at 20 and 400 kHz. For our purposes only the last pole is relevant

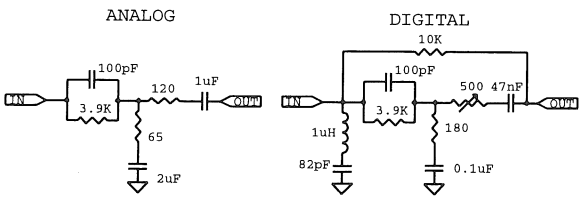

Fig. 7. Loop filters used for the analog PD and the digital PFD. The first is a simple phase-advance ac coupled to the diode laser. The second has an extra notch filter tuned at $\nu_0/2$ and a capacitor to increase the low-frequency gain. The resistor in parallel to the phase advance improves relocking

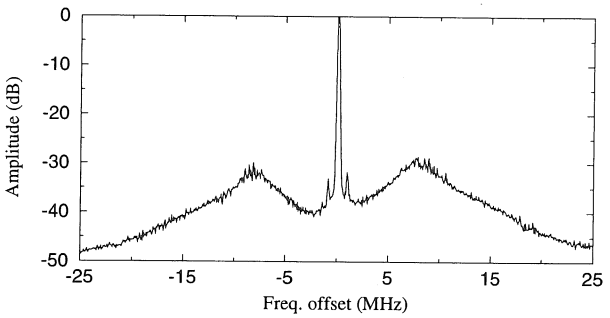

Fig. 8. Closed-loop beat note using the analog PD. The resolution bandwidth is 100 kHz

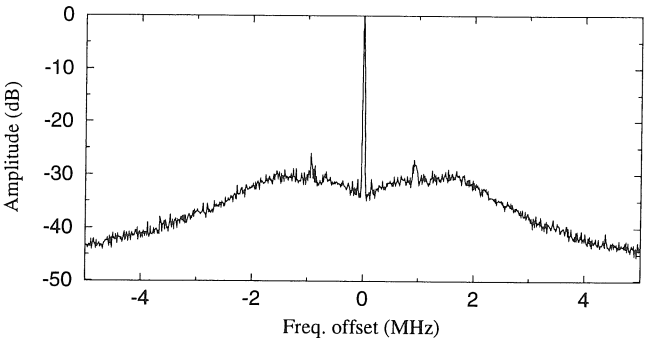

Fig. 9. Closed-loop beat note using the digital PFD. The resolution bandwidth is 10 kHz

$S_w = 48 \times 10^3$ Hz^2/Hz, we get $\eta = 0.96$, which corresponds to a value of $\langle\varphi^2\rangle$ of 0.04 rad^2. Using (5) and the fitted parameters for white and Lorentzian frequency noise, we obtain the calculated value $\langle\varphi^2\rangle = 0.035$ rad^2. The locking time, supposing optimum laboratory conditions, can be of the order of one hour. By adopting more complicated loop filters and increasing the LO frequency, it is possible to obtain a loop bandwidth in excess of 20 MHz.

For the digital PFD, since the delay is much larger, we have to limit the bandwidth to about 1.7 MHz (Fig. 9). The loop filter is again shown in Fig. 7. We have added to the simple phase-advance circuit a notch filter tuned to $\nu_0/2$, which is the main spurious component generated by the circuit. In addition, an extra resistor provides a dc path that makes relocking easier, and a capacitor increases the low-frequency gain. DC coupling of the injection current can damage or destroy the laser and therefore must be done carefully.

With this setup, we measured $\eta = 0.83$, $\langle\varphi^2\rangle = 0.19$ rad^2, while the computed value for $\langle\varphi^2\rangle$ is 0.15 rad^2. We also observed $|\bar{\Phi}^1(\nu)|^2$ under lock conditions up to 100 kHz using a FFT analyzer connected to the output of the PFD. The result was white phase noise with $S_\varphi \simeq 1 \times 10^{-7}$ rad^2/Hz. The expected value can be obtained from the low-frequency limit of the integrand in (5): $S_\varphi = (S_L + S_w)/\nu_u^2$, from which $S_\varphi = 0.43 \times 10^{-7}$ rad^2/Hz. With the digital PFD, the locking time is basically limited by the drift of the lasers, which, after a few hours, require some adjustment of the injection current in order not to jump to a different longitudinal mode. The tolerance to acoustic noise and vibration is much better than with the analog PD.

In order to reduce the delay, we put both an analog and a fast digital (a simple XOR gate) PD in parallel with the PFD. In this way we add to the linear phase response an oscillatory one, either a sine wave or a sawtooth. If the gain of the fast PD is not too high, the overall response is still monotonic but it is stepped. Properly adjusting the offset at the input of the integrator driving the PZT, it is possible to use a steep part in the curve. Using the XOR, we were able to increase the bandwidth to about 3 MHz. The analog mixer offered even better performance, but we felt that the additional complexity was unnecessary. Although the phase error is decreased, the extra PD reduces the reliability of the setup.

After some time, depending on the stability of the PZT voltage, the detector response will drift away from the steep slope. It is then necessary to monitor the beat note and, periodically, to adjust the PZT offset.

7 Applications in a frequency chain

The possibility of slip–free phase locking which can withstand a significant RMS phase deviation $\langle\varphi^2\rangle$ allows the realization of OPLLs, suitable for metrological applications, where the loop bandwidth is a fraction of the linewidth of the sources. To prove this, we have measured $\sigma(t)$, using artificially reduced values of ν_u.

We discuss, first, the results to be expected. If ν_u is small enough, we can neglect the delay and $D(\nu)$ in (4); moreover, the loop filter can be just a resistor. The loop is then of the first order and we have $\langle\varphi^2\rangle = \pi(S_L + S_w)/\nu_u$, while $\sigma^2(t)$ is given exactly by (25).

For five values of ν_u, we measured $\sigma(t)$ for eight different t, from 0.05 to 10 s in a 1–2–5 sequence. The data were then

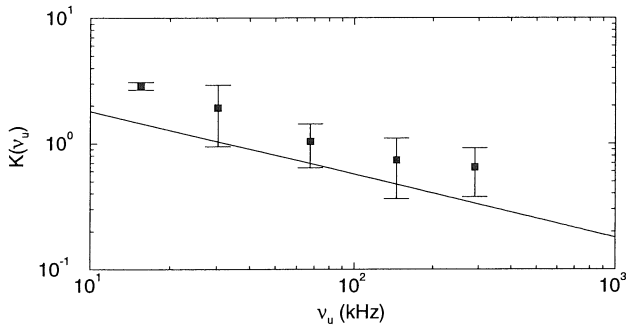

Fig. 10. Measured value of $K(\nu_u)$ vs ν_u. The *solid line* was calculated using (25)

fitted with $\sigma(t) = K(\nu_u)/t$, thereby determining the value of $K(\nu_u)$. In Fig. 10, $K(\nu_u)$ is plotted versus ν_u together with the curve computed using (25) and the values of S_w and S_L determined from the rf spectrum. These data are consistent with the closed-loop measurement of S_φ: they both show, however, that at very low frequencies our estimate of the frequency noise is about a factor 2 too small.

Only in the case $\nu_u \simeq 320$ kHz, where $\langle\varphi^2\rangle \simeq 1.2$, could we clearly observe a carrier in the beat note, while for smaller values of ν_u we obtained data similar to Fig. 1, which was actually recorded while measuring the second point in Fig. 10.

We see from Fig. 10 that, with $\nu_u \simeq 68$ kHz, it is possible to have $\sigma(1) \simeq 1$ Hz, which means $\sigma_y(1) \simeq 2.5 \times 10^{-15}$ for lasers at 850 nm. In contrast, letting $\langle\varphi^2\rangle \simeq 5.7$, $\nu_u = 68$ kHz and using (28) we have, for an analog loop under the same conditions, a cycle slip every 16 μs, so $\sigma_y(1) \simeq 1.7 \times 10^{-10}$. This "mild" phase locking is not simply easier and acceptable; it could even be desirable in chains where the multiplied phase noise of the low-frequency stages produces a larger linewidth than the slave laser or other transfer oscillators.

This tolerance to phase fluctuations can also be used for locking on low S/N beat notes. If we set τ for the minimum $\langle\varphi^2\rangle$ in (27), then, with $S_w \simeq 100$ kHz and $\langle\varphi^2\rangle \approx 6$, τ could be as low as 1130 with $\nu_u = 57$ kHz (i.e., 21 dB in 10 kHz bandwidth). Because the analog–to–TTL converter requires a minimum S/N ratio to operate properly, these numbers are not realistic. Although quantitative measurements are rather difficult, our feeling is that the digital PFD can operate with a S/N 10 dB less than the analog circuit in our typical experimental conditions. The reduction in minimum-required S/N could be very useful in schemes where weak beat notes are expected, as in optical comb generators or ultrafast detectors.

8 Conclusions

We have outlined an easy design procedure for OPLLs that gives acceptable agreement between computed and actual values. Using this procedure, we have built an OPLL with a bandwidth of about 8 MHz, obtaining a residual RMS phase noise of 0.2 rad and 0.96 of the power in the carrier, starting from two lasers with a beat note FWHM of more than 500 kHz. By choosing a higher LO frequency, the loop bandwidth could be at least 15 MHz.

Using a digital PFD with a linear range of more than ± 100 rad and a capture range of 70 MHz, it was necessary to reduce the loop bandwidth to less than 2 MHz in the simplest configuration or to 3 MHz in a slightly more complex case; these could be improved by adopting faster electronics. The disadvantages of the digital PD are compensated by the stability of operation (a locking time of hours is routinely achieved), the absence of cycle slips, and the tolerance of small S/N ratios.

We have measured the Allan variance $\sigma(t)$ of weakly locked lasers, where the loop bandwidth is a fraction of the linewidth. With a bandwidth as low as 15 kHz, a fifteenth of the HWHM of our beat note, we observed $\sigma_y(t) = 8 \times 10^{-15}$. The results agree with our simple theory and show that, without cycle slips, it is possible to obtain values of $\sigma(t)$ acceptable for a frequency chain. This opens the possibility of using broader (i.e., simpler or higher power) sources for frequency measurements in the visible, based on schemes such as divider stages or optical comb generators.

Acknowledgements. MP and TF acknowledge with gratitude financial support from the European Community's HCM and SCIENCE programmes during the course of this work.

References

1. F. Schmidt-Kaler, D. Leibfried, S. Seel, C. Zimmermann, W. König, M. Weitz, T. W. Hänsch: Phys. Rev. A (submitted)
2. T. Andreae, W. König, R. Wynands, D. Leibfried, F. Schmidt-Kaler, C. Zimmermann, D. Meschede, T. W. Hänsch: Phys. Rev. Lett. **69**, 1923 (1992)
3. F. Nez, M. D. Plimmer, S. Bourzeix, L. Julien, F. Biraben, R. Felder, O. Acef, J. J. Zondy, P. Laurent, A. Clairon, M. Abed, Y. Millerioux, P. Juncar: Phys. Rev. Lett. **69**, 2326 (1992)
4. K. Nakagawa, M. Kourogi, M. Ohtsu: Appl. Phys. B **57**, 425 (1993)
5. H. U. Daniel, M. Steiner, H. Walther: Appl. Phys. B **26**, 189 (1981)
6. O. Acef, L. Hilico, M. Bahoura, F. Nez, P. De Natale: Opt. Commun. **109**, 428 (1994)
7. M. Kourogi, K. Nakagawa, M. Ohtsu: IEEE J. QE-**29**, 2693 (1993)
8. R. Wynands, T. Mukai, T. W. Hänsch: Opt. Lett. **17**, 1749 (1992)
9. B. Dahmani, L. Hollberg, R. Drullinger: Opt. Lett. **12**, 876 (1987)
10. C. Shin, M. Ohtsu: IEEE J. QE-**29**, 374 (1993)
11. H. Telle, H. Li: Electron. Lett. **26**, 858 (1990)
12. S. Swartz, J. L. Hall, K. E. Gibble, D. S. Weiss: J. Opt. Soc. Am. B (submitted)
13. G. Santarelli, A. Clairon, S. N. Lea, G. M. Tino: Opt. Commun. **104**, 339 (1994)
14. C. Audoin: In *Metrology and Fundamental Constants*, ed. by A. F. Milone, P. Giacomo, F. Leschiutta, Int'l School of Physics E. Fermi, corso 68 (North–Holland, Amsterdam 1980)
15. M. Zhu J. L. Hall: J. Opt. Soc. Am. B **10**, 802 (1993)
16. D. C. Champeney: *Fourier Transforms and Their Physical Applications* (Academic, New York 1973)
17. K. Petermann: *Laser Modulation and Noise* (Kluwer, Dordrecht 1991)
18. P. Laurent, A. Clairon, C. Bréant: IEEE J. QE-**25**, 1131 (1989)
19. Z. Schuss: *Theory and Applications of Stochastic Differential Equations* (Wiley, New York 1980)
20. J. L. Hall, M. Long-Sheng, G. Kramer: IEEE J. QE-**23**, 427 (1987)